Resolving Nonperturbative Renormalization of a Microwave-Dressed Weakly Anharmonic Superconducting Qubit Coupled to a Single Quantized Mode

Ann, Byoung Moo; Deve, Sercan; Steele, Gary A.

Important note
To cite this publication, please use the final published version (if applicable).
Please check the document version above.

Resolving Nonperturbative Renormalization of a Microwave-Dressed Weakly Anharmonic Superconducting Qubit Coupled to a Single Quantized Mode

Byoung-moo Ann[1,2,*] Sercan Deve[1] and Gary A. Steele[1]

[1]*Kavli Institute of Nanoscience, Delft University of Technology, 2628 CJ Delft, The Netherlands*
[2]*Quantum Technology Institute, Korea Research Institute of Standards and Science, 34113 Daejeon, South Korea*

Microwave driving is a ubiquitous technique for superconducting qubits, but the dressed states description based on the conventionally used perturbation theory cannot fully capture the dynamics in the strong driving limit. Comprehensive studies beyond these approximations applicable to transmon-based circuit quantum electrodynamics (QED) systems are unfortunately rare, as the relevant works have been mainly limited to single-mode or two-state systems. In this work, we investigate a microwave-dressed transmon coupled to a single quantized mode over a wide range of driving parameters. We reveal that the interaction between the transmon and resonator as well as the properties of each mode is significantly renormalized in the strong driving limit. Unlike previous theoretical works, we establish a nonrecursive and non-Floquet theory beyond the perturbative regimes, which excellently quantifies the experiments. This work expands our fundamental understanding of dressed cavity QED-like systems beyond the conventional approximations. Our work will also contribute to fast quantum gate implementation, qubit parameter engineering, and fundamental studies on driven nonlinear systems.

Dynamically driving systems is a common methodology in physics [1–9]. Qubits or oscillators driven by time-periodic potentials are the most typical type of such systems. In circuit quantum electrodynamics (QED) platforms, a prototypical system for exploring and understanding light-matter interactions in the quantum regime [10], applying time-periodic potentials through charge or flux lines is a major means to perform quantum gate operations [11–19] or engineer the qubit's properties *in situ* [20–23].

In the strong driving limit, the significantly renormalized eigenbasis of multilevel qubits cannot be captured by low-order perturbation theory (PT) and two-state (TS) description. These can modify the quantum dynamics quantitatively and qualitatively. Unfortunately, investigating circuit QED or even general cavity QED-like systems in this direction has remained unexplored, although periodically driven quantum systems in the strong drive limit have been explored in various platforms [24–41].

Here, we perform a study on the renormalization of a transmon [42] coupled to a resonator. In-depth investigations of the driven transmon-resonator configuration have been intensively performed [43–50]. Recently, the efforts to break conventional approximations are also being actively reported [51–60]. Unlike most of the previous studies, we derive a nonrecursive and non-Floquet formula, advantageous for multilevel systems and nonperturbative problems. We identify a nonperturbatively modified qubit-resonator interaction in the experiments through Lamb shifts and cross-nonlinearities. The theory is cross-checked through the observed renormalized Rabi frequencies and energy

relaxation times. We clearly see the breakdowns of the PT and TS model as well as rotating wave approximation.

Theoretical description.—The Hamiltonian of a bare transmon reads $\hat{H}_q = 4E_C(\hat{N} - N_g) - E_J \cos \hat{\phi}(E_J \gg E_C)$, where E_C, E_J, and N_g are the charging, Josephson energies, and offset charges, respectively. $\hat{N}$ and $\hat{\phi}$ are the Cooper-pair number and phase operators, respectively. Let us set E_n and $|n\rangle_q$ as the nth eigenvalue and eigenstate, respectively, of $\hat{H}_q$. The fundamental transition frequency and self-nonlinearity of the transmon is then given by $\omega_q = E_1 - E_0$ and $\chi_q = \omega_q - (E_2 - E_1)$. We define $\hat{d}$ as a normalized dipole operator given by $\eta \hat{N}$, where $\eta = -i(32E_C/E_J)^{1/4}$ (see Supplemental Material, Sec. A1 [61]). It is important to note that $\hat{d}$ is an anti-Hermitian operator.

A microwave drive adds an additional term $\hat{H}_d(t) = \Omega_d \hat{d} \sin \omega_d t$. Here, Ω_d and ω_d are the drive amplitude and frequency, respectively. We then invoke a unitary operator $\hat{U}_q(t)$ that satisfies $\hat{U}_q(t)[\hat{H}_q + \hat{H}_d(t) - i\partial/\partial t]\hat{U}_q^\dagger(t) = \hat{K}_q$, where $\hat{K}_q$ denotes an effective static "Kamiltonian," which captures only the slow dynamics of the system. The nth eigenenergies of $\hat{K}_q$ will be expressed by $\tilde{E}_n$. $\hat{K}_q$ should be set such that $\tilde{E}_n$ is adiabatically connected to E_n as $\Omega_d \to 0$. It is also useful to define the renormalized dipole elements $\tilde{d}_{nm}^{(\pm)}$, which satisfy (see Supplemental Material, Secs. A1 and A2 [61])

$$\hat{U}_q(t)\hat{d}\hat{U}_q^\dagger(t) \cong \sum_{n,m} \mp \tilde{d}_{nm}^{(\pm)} e^{i(m-n\pm1)\omega_d t}\hat{\sigma}_{nm}. \quad (1)$$

TABLE I. Hamiltonians and their effective static forms used in this work. See the main text for their definitions.

Hamiltonian	Effective static form
$\hat{H}_q + \hat{H}_d(t)$	$\hat{K}_q$
$\hat{K}_q + \hat{H}_I + \hat{H}_r$	$\hat{K}_1$
$\hat{K}_q + \hat{\tilde{H}}_{SI} + \hat{H}_r$	$\hat{K}_2$
$\hat{H}_q + \hat{H}_d(t) + \hat{H}_I + \hat{H}_r$ $(\hat{K}_q + \hat{\tilde{H}}_I + \hat{H}_r)$	$\hat{K}$
$\hat{H}_{TS} + \hat{H}_{d,TS}(t) + \hat{H}_{I,TS} + \hat{H}_r$	$\hat{K}_{TS}$

Here, $\hat{\sigma}_{nm} = |n\rangle_q\langle m|_q$. The sign distinguishes whether the elements originally concern the absorption or emission processes. Equation (1) concerns the renormalization of Rabi frequencies and energy relaxation times.

The renormalization can also be explored for the interaction between a microwave-dressed transmon and the quantized field of a dispersively coupled readout resonator. We define $\hat{H}(t)$ like below:

$$\hat{H}(t) = \hat{H}_q + \hat{H}_d(t) + \underbrace{\omega_r \hat{a}^\dagger \hat{a}}_{\hat{H}_r} + \underbrace{g\hat{d}(\hat{a} - \hat{a}^\dagger)}_{\hat{H}_I}. \quad (2)$$

Here, $\hat{a}$ and ω_r denote the field operator and frequency of the resonator, respectively. $\hat{H}_I$ denotes the interaction between the transmon and resonator. g refers to the coupling constant. The renormalization of the transmon-resonator interaction can be nicely captured by the expression below:

$$\hat{U}_q \hat{H}(t) \hat{U}_q^\dagger = \hat{K}_q + \omega_r \hat{a}^\dagger \hat{a} + \underbrace{g[\hat{U}_q \hat{d}\hat{U}_q^\dagger](\hat{a} - \hat{a}^\dagger)}_{\hat{\tilde{H}}_I}. \quad (3)$$

The effects of the renormalized interaction terms ($\hat{\tilde{H}}_I$) and renormalized bare transmon ($\hat{K}_q$) are disentangled in Eq. (3), whereas they have been ambiguated in the theoretical descriptions of previous works [52]. We better define $\hat{\tilde{H}}_{SI}$ by collecting only the static components of $\hat{\tilde{H}}_I(t)$ to distinguish purely static effects from $\hat{\tilde{H}}_I(t)$. We also define $\hat{K}$ as an effective static form of $\hat{H}(t)$, related by $\hat{U}(t)$ satisfying $\hat{K} = \hat{U}(t)[\hat{H}(t) - i\partial/\partial t]\hat{U}^\dagger(t)$. See Supplemental Material Sec. A3 [61] for how to derive $\hat{U}(t)$.

Table I summarizes all the Hamiltonian models and their effective static forms used in this work. $\hat{K}_1$ and $\hat{K}_2$ describe the transmon-resonator system with interaction terms $\hat{H}_I$ and $\hat{\tilde{H}}_{SI}$, respectively. We also define a corresponding TS system by $\hat{H}_{TS} = (\omega_{0,TS}/2)\hat{\sigma}_z$. Its interaction with the resonator is expressed by $\hat{H}_{I,TS} = g_{TS}\hat{\sigma}_x(\hat{a} + \hat{a}^\dagger)$.

Experimental results and analysis.—A graphical description of this system is presented in Fig. 1(a), which
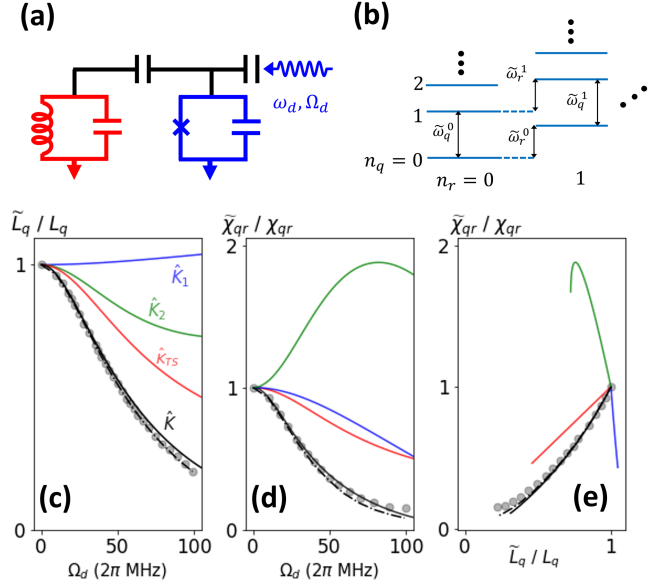

FIG. 1. Renormalized interaction between the transmon (blue) and resonator (red) for $\omega_d/2\pi = 5.89$ GHz. (a),(b) Circuit and energy level diagrams. A blue wavy arrow indicates a microwave drive to the transmon. (c)–(e) Lamb shift ($\tilde{L}_q$) and cross-nonlinearity ($\tilde{\chi}_{qr}$) divided by the unnormalized values (L_q, χ_{qr}). ω_d is 5.89 GHz in the experiment. Circles: experimental data. Black, blue, green, and red solid lines refer to theoretical calculations based on $\hat{K}$, $\hat{K}_1$, $\hat{K}_2$, and $\hat{K}_{TS}$, respectively. The dashed line refers to fully numerical calculation based on Eq. (2). See Table I and the corresponding main text for the description of each model. Statistical errors in data are negligible and, thus, not presented in the plots.

shows a dispersively coupled microwave-dressed transmon (blue) and resonator (red). Figure 1(b) shows the energy diagram of $\hat{K}$. The energy levels are probed through resonator transmission and qubit two-tone spectroscopy. The resonator is used to read out the qubit states in the two-tone spectroscopy. See Supplemental Material Sec. E [61] for the details. Here, $n_{q,r}$ denote the excitation numbers of the transmon and resonator, respectively. Each horizontal line represents an eigenstate of $\hat{K}$. $\tilde{\omega}_q^{n_r}$ ($\tilde{\omega}_r^{n_q}$) refers to the transmon (resonator) frequency when the resonator (transmon) is in the n_r (n_q) energy state. We additionally introduce symbols $L_q = \omega_q^0 - \omega_q$ and $\chi_{qr} = \omega_q^0 - \omega_q^1$, which refer to the Lamb shift and cross-nonlinearity in the fundamental transition of the transmon. From the two-tone spectroscopy [70,71], we observe $\omega_q^0/2\pi = 5.867$ GHz, $\omega_r^0/2\pi = 4.289$ GHz, $\chi_q^0/2\pi = 149$ MHz, and $\chi_{qr}/2\pi = 6$ MHz. From this observation, we extract the parameters $E_J/2\pi = 28.6$ GHz, $E_C/2\pi = 149$ MHz, $\omega_r/2\pi = 4.334$ GHz, $g/2\pi = 245$ MHz, and $L_q/2\pi = 33$ MHz. Both $\omega_{0,TS}$ and g_{TS} in $\hat{H}_{TS}$ are properly adjusted such that they yield the same χ_{qr}, ω_q^0, and ω_r^0 compared to those of the transmon.

In Figs. 1(c)–1(e), we present experimentally observed Lamb shifts and cross-nonlinearities of the transmon from two-tone spectroscopy. $\omega_d/2\pi$ is 5.89 GHz, sufficiently near $\omega_q^0/2\pi$. We explore both renormalized cross-nonlinearity and Lamb shift, denoted by $\tilde{\chi}_{qr}$ and $\tilde{L}_q$, in Figs. 1(c)–1(e). $\tilde{\chi}_{qr}$ alone is not sufficient to fully comprehend the renormalized interaction between the transmon and resonator, since it also largely depends on $\tilde{\chi}_q$. Since $\tilde{L}_q$ is almost independent of $\tilde{\chi}_q$, it can be used to investigate the renormalization effects that originate from the transmon-resonator interaction.

The discrepancy between the predictions by the $\hat{K}_1$ model (blue lines) and the experimental data indicates significant renormalization of $\hat{H}_I$. This can be translated to the breakdown of the low-order PT, which assumes negligible renormalization of the eigenbasis. The difference between the green line ($\hat{K}_2$) and experimental data throughout Figs. 1(c)–1(e) strongly suggests that dynamical components in $\hat{H}_I$ have significant effects. The approximation used in $\hat{K}_{1,2}$ often appears when describing the interaction among quantized modes even in the recent studies [47–50]. In addition, we separately discuss the effect of the rotating wave approximation in Supplemental Material, Sec. A5 [61].

Although the transmon-drive detuning $\Delta_{qd}^0/2\pi = 23$ MHz is substantially smaller than the self-nonlinearity $\chi_q^0/2\pi = 149$ MHz, the experimental results deviate remarkably from the predictions based on a driven TS system (red lines). We confirm that the ratio between L_q and χ_{qr} is invariant with respect to drive fields as seen in the red lines ($\hat{K}_{TS}$) in Figs. 1(c)–1(e). This shows negligible dynamical effects for the TS system under drive fields.

For dressed TS systems, dynamical effects are expected to be negligible unless $\tilde{d}_{10} \sim d_{01}$ or ω_d meets the matching conditions for two-photon sideband transitions (Supplemental Material Sec. A4 [61]). For transmons, there are possibilities for the fundamental transition to be affected by the dynamical part of $\hat{\tilde{H}}_I$ due to the higher energy levels. Particularly, the diagonal elements of the renormalized dipole matrix $\tilde{d}_{nn}$ are the major contribution in the case of near-resonant drive fields. For a TS system, $|\tilde{d}_{00}| = |\tilde{d}_{11}|$ always holds, and, therefore, the dynamical effects originating from these components do not induce any energy level shift. For a transmon, however, $|\tilde{d}_{00}| \neq |\tilde{d}_{11}|$ due to higher energy levels, and then one should also seriously take the diagonal elements into consideration. See Supplemental Material Sec. C [61] for the calculated $\tilde{d}_{nn}$.

In Fig. 2, we present the observed Lamb shifts (a) and cross-nonlinearities (b) as functions of corresponding Stark shifts ($\delta\omega_q^0 = \tilde{\omega}_q^0 - \omega_q^0$) for various ω_d from near- to far-off-resonant regimes. The investigated range of drive amplitudes are regulated differently for each ω_d, such that the
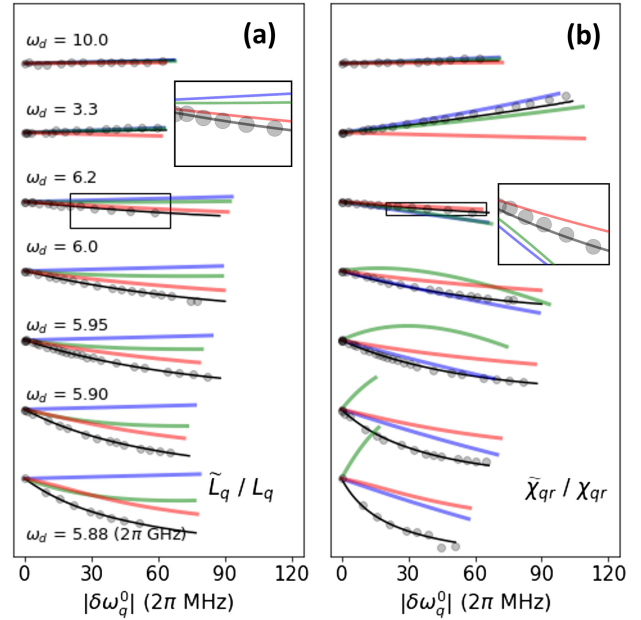

FIG. 2. Renormalized interaction between the transmon and resonator with various ω_d. We present renormalized Lamb shifts $\tilde{L}_q$ and cross-nonlinearities ($\tilde{\chi}_{qr}$) for given absolute values of Stark shifts ($|\delta\omega_q^0| = |\tilde{\omega}_q^0 - \omega_q^0|$). The circles refer to the observed Lamb shifts and cross-nonlinearities. Theoretical calculations based on several models are denoted by lines. The color legend is identical to that in Fig. 1. Insets give magnified views of the areas enclosed by the boxes. Various tendencies can be seen with respect to the transmon-drive detunings. See the main text for detailed descriptions. Errors in data are negligible and, thus, not presented in the plots.

ranges of $|\delta\omega_q^0/2\pi|$ become similar. The theoretical model based on $\hat{K}$ (black lines) agrees well with the experimental values (circles) for all ω_d. Meanwhile, theories based on $\hat{K}_{TS}$ (red), $\hat{K}_1$ (blue), and $\hat{K}_2$ (green) fail to explain the experimental data, in general. We do not use any free fitting parameter in all the theoretical plots.

For large detunings ($\omega_d/2\pi = 3.3$ and 10 GHz), the $\hat{K}_1$ model nicely explains the experiments, suggesting $\hat{H}_I \approx \hat{\tilde{H}}_I$. As ω_d approaches ω_q^0, we can clearly see that the deviation of the $\hat{K}_1$ model from the experimental data grows significantly. When $\omega_d/2\pi$ is near 6.0 GHz, however, we see an exception for the cross-nonlinearities. We attribute this coincidence to the dynamical effects. It is interesting to remark that the data with $\omega_d/2\pi = 3.3$ GHz exhibit significant renormalization of the cross-nonlinearities but not of the Lamb shifts. This suggests that the change in $\tilde{\chi}_{qr}$ for $\omega_d/2\pi = 3.3$ GHz mainly originates from the change in $\tilde{\chi}_q$. It is also beneficial to discuss the discrepancy between the predictions from the two-state model and the experiment results. For large $|\Delta_{qd}|$ ($\omega_d/2\pi = 3.3$ and 10 GHz), both $\tilde{L}_q$ and $\tilde{\chi}_{qr}$ are nearly invariant from the TS model, indicating

$\tilde{\tilde{H}}_{I,\mathrm{TS}} \approx \hat{H}_{I,\mathrm{TS}}$ under the investigated range of drive amplitudes. The discrepancy becomes larger when $|\Delta_{qd}| \to 0$, and this result is already expected from Fig. 1. For $\omega_d/2\pi = 5.88$ GHz, the corresponding $\Delta_{qd}/2\pi$ is only 13 MHz, which is tenfold smaller than χ_q^0. Nonetheless, we still see the dramatic failure of the $\hat{K}_{\mathrm{TS}}$ model.

In the following, we investigate the renormalization effects using different approaches, through Rabi frequencies and coherence properties of the transmon. When we introduce an additional Rabi tone that induces resonant transitions $\widetilde{|0\rangle} \leftrightarrow \widetilde{|1\rangle}$ of the dressed transmon, the Rabi frequency $\tilde{\Omega}_R$ satisfies

$$\tilde{\Omega}_R = 2 \underbrace{\sqrt{\frac{\kappa_{\mathrm{ex}}(\tilde{\omega}_q^0)\gamma(\tilde{\omega}_q^0)P_R}{\tilde{\omega}_q^0}}}_{\Gamma} \times \tilde{d}_{01}^{0(-)}. \qquad (4)$$

Here, $\tilde{d}_{nm}^{k(\pm)}$ are matrix components of $\hat{U}(t)\hat{d}\hat{U}^\dagger(t)$ when $n_r = k$. We assume that the frequency of the Rabi tone is adjusted to $\tilde{\omega}_q^0$ for resonant Rabi oscillations. P_R is the power of the Rabi tone measured at the output of the microwave source, κ_{ex} refers to the transmon's external coupling to the drive line, and γ is the transfer function between the microwave source and device. Both κ_{ex} and γ are unknown without additional calibrations.

In Fig. 3(a), we present $\tilde{\Omega}_R$ for $\omega_d/2\pi = 10$ GHz (gray circles) with respect to absolute values of Stark shifts ($|\delta\omega_q| = |\tilde{\omega}_q^0 - \omega_q^0|$). The dashed line refers to the Rabi
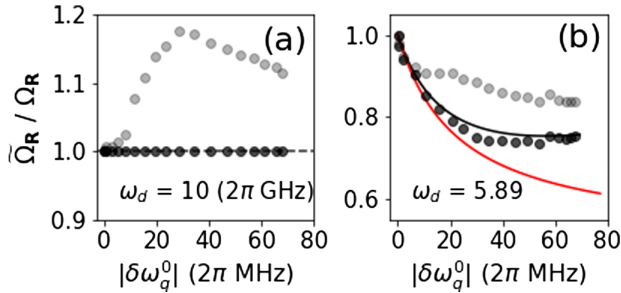

FIG. 3. Renormalized Rabi frequencies ($\tilde{\Omega}_R$) for given $|\delta\omega_q^0|$. Here, Ω_R indicates the Rabi frequency when $\Omega_d = 0$. (a) $\tilde{\Omega}_R/\Omega_R$ versus $|\delta\omega_q^0|$ for $\omega_d/2\pi = 10$ GHz. The gray circles refer to the observed values. When $\Gamma = 1$, $\tilde{\Omega}_R \approx \Omega_R$ should hold for large-detuned drive fields for both the transmon and TS system (dashed line). Based on this, we extract the experimental Γ and obtain black circles that correspond to the gray circles. (b) $\tilde{\Omega}_R/\Omega_R$ versus $|\delta\omega_q^0|$ for $\omega_d/2\pi = 5.89$ GHz. We divide the observed values (gray circles) by the experimental Γ [Eq. (4)] obtained from (a) and obtain corrected values with $\Gamma = 1$ (black circles). The solid lines refer to the approximate theoretical curves under $\Gamma = 1$. The black and red lines denote transmon and TS system theories, respectively. Errors in data are negligible and, thus, not presented in the plots.

frequencies when $\Gamma = 1$ for both the transmon and TS models. For such far-off-resonant drive fields, under the explored range of ac Stark shifts, the renormalization of the transmon's dipole elements is negligible as found in Fig. 2 for both the transmon and TS models. Hence, the changes in $\tilde{\Omega}_R$ should be attributed to the changes in Γ. Based on this, we can extrapolate the experimental Γ. By dividing the measured data by the experimental Γ, we obtain the dark circles in Fig. 3(a). In Fig. 3(b), we explain the data with $\omega_d/2\pi = 5.89$ GHz by using the same experimental Γ as in Fig. 3(a). In Fig. 3(b), the corrected values (dark circles) show a much better agreement with transmon-based theory than TS theory.

The theoretical investigation of renormalization of transmon coherence times is reported recently [59] for sufficiently off-resonant drive fields using perturbative expansion. In this work, we obtain the nonperturbative solution by applying $\hat{U}_q$ to $\hat{H}_{\mathrm{st}} = \lambda_\parallel(t)\hat{n} + \lambda_\perp(t)\hat{d}$ that describes the interaction between the system and noise environment. Please recall that we did the same job for $\hat{H}_I$ to resolve the renormalized Lamb shift and cross-nonlinearities. $\hat{n} = \sum_i \sqrt{i+1}|i\rangle_q\langle i|_q$ is the transmon number operator. $\lambda(t)$ is a stochastic variable describing the environmental noise. We find the relations below (see Supplemental Material Sec. B [61]):

$$\frac{1}{\tilde{T}_1} = \pi\left[S_{\lambda_\perp}(\tilde{\omega}_q^0)(\tilde{d}_{01}^{0(-)2})\right],$$

$$\frac{1}{\tilde{T}_\varphi} = \pi\left[S_{\lambda_\parallel}(0)(\tilde{n}_{11}^0 - \tilde{n}_{00}^0)^2 + S_{\lambda_\perp}(\omega_d)(\tilde{d}_{11}^{0(-)} - \tilde{d}_{00}^{0(-)})^2\right].$$

$$(5)$$

$\tilde{T}_2$ is the renormalized pure dephasing time satisfying $\tilde{T}_2^{-1} = (2\tilde{T}_1)^{-1} + \tilde{T}_\varphi^{-1}$. Here, $S_\lambda(\omega) = (1/2\pi)\int d\tau e^{-i\omega\tau} \times \langle\lambda^*(t)\lambda(t+\tau)\rangle$. $\tilde{n}_{nm}^k$ are the matrix elements of $\hat{\tilde{n}} = \hat{U}\hat{n}\hat{U}^\dagger$, when $n_r = k$. Only the fluctuations in the transmon's resonant frequency are taken into account in this expression. Equation (5) becomes identical to Eqs. (42) and (45) in Ref. [38] in the two-state approximation.

In Fig. 4(a), we present $\tilde{T}_1/T_1$ with respect to $|\delta\omega_q^0|$ for $\omega_d/2\pi = 10$ GHz (circles). The theoretical estimation under the ideal situation ($S_{\lambda_\perp} = \mathrm{const}$) is given by the gray dashed line. The flatness of the gray line is due to the fact that $\tilde{d}_{01}^{0(-)} \approx d_{01}^{0(-)}$ should hold for far-of-resonant drive fields. Thereby, we can draw a conclusion that the change in $\tilde{T}_1/T_1$ is attributed to the ω_q^0 dependence of $S_{\lambda_\perp}$. Therefore, we can extrapolate $S_{\lambda_\perp}(\tilde{\omega}_q^0)/S_{\lambda_\perp}(\omega_q^0)$ by low-order polynomial fitting (dark dashed line). Based on this extrapolation, we fit the data with $\omega_d/2\pi = 5.89$ GHz in Fig. 4(b). Unfortunately, we cannot thoroughly verify the second equation in Eq. (5) due to experimental limitations. See Supplemental Material Sec. F [61] for
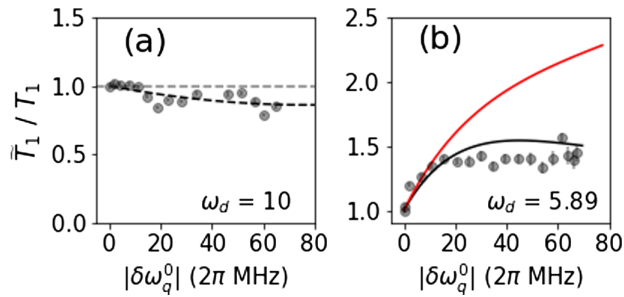
FIG. 4. Renormalized energy relaxation time ($\tilde{T}_1$) for given $|\delta\omega_q^0|$. (a) $\tilde{T}_1/T_1$ versus $|\delta\omega_q^0|$ is presented for $\omega/2\pi = 10$ GHz. The gray dashed line is a theoretical estimation when $S_{\lambda_\perp}$ is constant with respect to $\delta\omega_q^0$. The black dashed line is a polynomial fit up to second order. From this, we extrapolate $S_{\lambda_\perp}(\tilde{\omega}_q^0)$. (b) $\tilde{T}_1/T_1$ versus $|\delta\omega_q^0|$ for $\omega_d/2\pi = 5.89$ GHz. Black (transmon) and red (TS) lines refer to theoretical estimations considering nonconstant $S_{\lambda_\perp}(\tilde{\omega}_q^0)$.

our investigation on the renormalized dephasing times ($\tilde{T}_2$). See Supplemental Material Sec. G [61] for the calculated $\tilde{\Omega}_R$, $\tilde{T}_1$, and $\tilde{T}_2$ based on our formula with various drive frequencies.

Conclusion.—In summary, we have verified the non-perturbative renormalization of a coupled transmon-resonator system. The significant renormalization of the transmon-resonator interaction is identified from the changes of Lamb shifts and cross-nonlinearities. The results are also consistent with the renormalized Rabi frequencies and energy relaxation times observed separately. Without using recursive formulas and Floquet theory, we quantitatively explain the experiments. Our work represents a significant step from the previous relevant works confined to single-mode or two-state descriptions.

Although the performed experiments are confined to a weakly anharmonic circuit QED system, overall strategies to account for the renormalization will concern a broad range of cavity QED-like systems or, more generally, even to coupled multimode systems. Furthermore, transmons are also well-known examples of Duffing oscillators or pendulums in quantum regimes, and, thus, our work will also contribute to fundamental understanding on driven non-linear systems.

Data supporting the plots within this paper are available through Zenodo [72]. Further information is available from the corresponding author upon reasonable request.

*byoungmoo.ann@gmail.com

[1] Jon H. Shirley, Solution of the Schrödinger equation with a Hamiltonian periodic in time, Phys. Rev. B **97**, 138 (1965).

[2] Hideo Sambe, Steady states and quasienergies of a quantum-mechanical system in an oscillating field, Phys. Rev. A **7**, 2203 (1973).

[3] Pasi Lähteenmäki, G. S. Paraoanu, Juha Hassel, and Pertti J. Hakonen, Dynamical Casimir effect in a Josephson meta-material, Proc. Natl. Acad. Sci. U.S.A. **110**, 4234 (2013).

[4] André Eckardt, Colloquium: Atomic quantum gases in periodically driven optical lattices, Rev. Mod. Phys. **89**, 011004 (2017).

[5] T. Oka and S. Kitamura, Floquet engineering of quantum materials, Annu. Rev. Condens. Matter Phys. **10**, 387 (2019).

[6] N. Yao and C. Nayak, Time crystals in periodically driven systems, Phys. Today **71**, No. 9, 40 (2018).

[7] M. S. Rudner and N. H. Lindner, Band structure engineering and non-equilibrium dynamics in Floquet topological insulators, Nat. Rev. Phys. **2**, 229 (2018).

[8] H. Qiao, Y. P. Kandel, J. S. van Dyke, S. Fallahi, G. C. Gardner, M. J. Manfra, E. Barnes, and J. M. Nichol, Floquet-enhanced spin swaps, Nat. Commun. **12**, 2142 (2021).

[9] Ran He, Ming-Zhong Ai, Jin-Ming Cui, Yun-Feng Huang, Yong-Jian Han, Chuan-Feng Li, Guang-Can Guo, G. Sierra, and C. E. Creffield, Riemann zeros from Floquet engineering a trapped-ion qubit, npj Quantum Inf. **7**, 109 (2021).

[10] A. Blais, A. Grimson, S. M. Girvin, and A. Wallraf, Circuit quantum electrodynamics, Rev. Mod. Phys. **93**, 025005 (2021).

[11] K. S. Kumar, A. Vepsäläinen, S. Danilin, and G. S. Paraoanu, Stimulated Raman adiabatic passage in a three-level superconducting circuit, Nat. Commun. **7**, 10628 (2016).

[12] P. J. Leek, S. Filipp, P. Maurer, M. Baur, R. Bianchetti, J. M. Fink, M. Göppl, L. Steffen, and A. Wallraff, Using sideband transitions for two-qubit operations in superconducting circuits, Phys. Rev. B **79**, 180511 (2009).

[13] P. J. Leek, M. Baur, J. M. Fink, R. Bianchetti, L. Steffen, S. Filipp, and A. Wallraff, Cavity quantum electrodynamics with separate photon storage and qubit readout modes, Phys. Rev. Lett. **104**, 100504 (2010).

[14] K. S. Kumar, A. Vepsäläinen, S. Danilin, and G. S. Paraoanu, Stimulated Raman adiabatic passage in a three-level super-conducting circuit, Nat. Commun. **7**, 10628 (2016).

[15] Matthew Reagor *et al.*, Demonstration of universal para-metric entangling gates on a multi-qubit lattice, Sci. Adv. **2**, 4 (2014).

[16] Antti Vepsäläinen, Sergey Danilin, and G. S. Paraoanu, Superadiabatic population transfer in a three-level super-conducting circuit, Sci. Adv. **2**, 5 (2019).

[17] Easwar Magesan and Jay M. Gambetta, Effective Hamiltonian models of the cross-resonance gate, Phys. Rev. A **101**, 052308 (2020).

[18] J. D. Strand, M. Ware, F. Beaudoin, T. A. Ohki, B. R. Johnson, A. Blais, and B. L. T. Plourde, First-order sideband interactions with flux-driven asymmetric transmon qubits, Phys. Rev. B **87**, 220505 (2013).

[19] S. Krinner, P. Kurpiers, B. Royer, P. Magnard, I. Tsitsilin, J.-C. Besse, A. Remm, A. Blais, and A. Wallraff, Demonstration of an all-microwave controlled-phase gate between far detuned qubits, Phys. Rev. Appl. **14**, 044039 (2020).

[20] Vera Gramich, Simone Gasparinetti, Paolo Solinas, and Joachim Ankerhold, Lamb-shift enhancement and detection in strongly driven superconducting circuit, Phys. Rev. Lett. **113**, 027001 (2014).

[21] Pranav S. Mundada, András Gyenis, Ziwen Huang, Jens Koch, and Andrew A. Houck, Floquet-engineered enhancement of coherence times in a driven fluxonium qubit, Phys. Rev. Appl. **14**, 054033 (2020).

[22] J. Long, H. S. Ku, X. Wu, X. Gu, R. E. Lake, M. Bal, Y.-x. Liu, and D. P. Pappas, Electromagnetically induced transparency in circuit quantum electrodynamics with nested polariton states, Phys. Rev. Lett. **120**, 083602 (2018).

[23] B. Ann and G. A. Steele, Tunable and weakly invasive probing of a superconducting resonator based on electromagnetically induced transparency, Phys. Rev. A **102**, 053721 (2020).

[24] D. A. Andrews and G. Newton, Observation of Bloch-Siegert shifts in the $2^2S_{1/2}$-$2^2P_{1/2}$ microwave resonance in atomic hydrogen, J. Phys. B **8**, 1415 (1975).

[25] William D. Oliver, Yang Yu, Janice C. Lee, Karl K. Berggren, Leonid S. Levitov, and Terry P. Orlando, Mach-Zehnder interferometry in a strongly driven superconducting qubit, Science **310**, 1653 (2005).

[26] C. M. Wilson, T. Duty, F. Persson, M. Sandberg, G. Johansson, and P. Delsing, Coherence times of dressed states of a superconducting qubit under extreme driving, Phys. Rev. Lett. **98**, 257003 (2008).

[27] G. D. Fuchs, V. V. Dobrovitski, D. M. Toyli, F. J. Heremans, and D. D. Awschalom, Gigahertz dynamics of a strongly driven single quantum spin, Science **326**, 5959 (2009).

[28] Jani Tuorila, Matti Silveri, Mika Sillanpää, Erkki Thuneberg, Yuriy Makhlin, and Pertti Hakonen, Stark effect and generalized Bloch-Siegert shift in a strongly driven two-level system, Phys. Rev. Lett. **105**, 257003 (2010).

[29] Chunqing Deng, Jean-Luc Orgiazzi, Feiruo Shen, Sahel Ashhab, and Adrian Lupascu, Observation of Floquet states in a strongly driven artificial atom, Phys. Rev. Lett. **115**, 133601 (2015).

[30] J. V. Koski, A. J. Landig, A. Pályi, P. Scarlino, C. Reichl, W. Wegscheider, G. Burkard, A. Wallraff, K. Ensslin, and T. Ihn, Floquet spectroscopy of a strongly driven quantum dot charge qubit with a microwave resonator, Phys. Rev. Lett. **121**, 043603 (2018).

[31] B. Ann, W. Kessels, and G. A. Steele, Two-photon sideband interaction in a driven quantum Rabi model: Quantitative discussions with derived longitudinal drives and beyond the rotating wave approximation, Phys. Rev. Res. **3**, 013005 (2022).

[32] Anthony Gandon, Camille Le Calonnec, Ross Shillito, Alexandru Petrescu, and Alexandre Blais, Engineering, control, and longitudinal readout of Floquet qubits, Phys. Rev. Appl. **17**, 064006 (2022).

[33] Peng Zhao, Teng Ma, Yirong Jin, and Haifeng Yu, Combating fluctuations in relaxation times of fixed-frequency transmon qubits with microwave-dressed states, Phys. Rev. Lett. **105**, 062605 (2022).

[34] S. Park, W. Lee, S. Jang, Y.-B. Choi, J. Park, W. Jung, K. Watanabe, T. Taniguchi, G. Y. Cho, and G.-H. Lee, Steady Floquet–Andreev states in graphene Josephson junctions, Nature (London) **603**, 421 (2022).

[35] Shunsuke Nishimura, Kohei M. Itoh, Junko Ishi-Hayase, Kento Sasaki, and Kensuke Kobayashi, Demonstration of Floquet engineering using pulse driving in a diamond two-level system under a large-amplitude modulation, Phys. Rev. Appl. **18**, 064023 (2022).

[36] Arne Laucht *et al.*, Breaking the rotating wave approximation for a strongly driven dressed single-electron spin, Phys. Rev. B **94**, 161302(R) (2017).

[37] Arne Laucht *et al.*, A dressed spin qubit in silicon, Nat. Nanotechnol. **12**, 61 (2017).

[38] G. Ithier *et al.*, Decoherence in a superconducting quantum bit circuit, Phys. Rev. B **72**, 134519 (2005).

[39] Yiying Yan, Zhiguo Lü, JunYan Luo, and Hang Zheng, Effects of counter-rotating couplings of the Rabi model with frequency modulation, Phys. Rev. A **96**, 033802 (2017).

[40] Maxime Boissonneault, J. M. Gambetta, and Alexandre Blais, Improved superconducting qubit readout by qubit-induced nonlinearities, Phys. Rev. Lett. **105**, 100504 (2010).

[41] Lev S. Bishop, Eran Ginossar, and S. M. Girvin, Response of the strongly driven Jaynes-Cummings oscillator, Phys. Rev. Lett. **105**, 100505 (2010).

[42] J. Koch, T. M. Yu, J. Gambetta, A. A. Houck, D. I. Schuster, J. Majer, A. Blais, M. H. Devoret, S. M. Girvin, and R. J. Schoelkopf, Charge-insensitive qubit design derived from the Cooper pair box, Phys. Rev. A **76**, 042319 (2007).

[43] I. Pietikäinen, J. Tuorila, D. S. Golubev, and G. S. Paraoanu, Photon blockade and the quantum-to-classical transition in the driven-dissipative Josephson pendulum coupled to a resonator, Phys. Rev. A **99**, 063828 (2019).

[44] I. Pietikäinen, S. Danilin, K. S. Kumar, J. Tuorila, and G. S. Paraoanu, Multilevel effects in a driven generalized Rabi model, J. Low Temp. Phys. **191**, 354 (2018).

[45] Andre Schneider, Jochen Braumüller, Lingzhen Guo, Patrizia Stehle, Hannes Rotzinger, Michael Marthaler, Alexey V. Ustinov, and Martin Weides, Local sensing with the multilevel ac Stark effect, Phys. Rev. A **97**, 062334 (2018).

[46] F. Beaudoin, M. P. da Silva, Z. Dutton, and A. Blais, First-order sidebands in circuit QED using qubit frequency modulation, Phys. Rev. A **86**, 022305 (2012).

[47] Maxime Boissonneault, A. C. Doherty, F. R. Ong, P. Bertet, D. Vion, D. Esteve, and A. Blais, Back-action of a driven nonlinear resonator on a superconducting qubit, Phys. Rev. A **85**, 022305 (2012).

[48] S. Zeytinoğlu, M. Pechal, S. Berger, A. A. Abdumalikov, Jr., A. Wallraff, and S. Filipp, Microwave-induced amplitude- and phase-tunable qubit-resonator coupling in circuit quantum electrodynamics, Phys. Rev. A **91**, 043846 (2015).

[49] B. K. Mitchell, R. K. Naik, A. Morvan, A. Hashim, J. M. Kreikebaum, B. Marinelli, W. Lavrijsen, K. Nowrouzi, D. I. Santiago, and I. Siddiqi, Hardware-efficient microwave-activated tunable coupling between superconducting qubits, Phys. Rev. Lett. **127,** 200502 (2021).

[50] K. X. Wei *et al.*, Hamiltonian engineering with multicolor drives for fast entangling gates and quantum crosstalk cancellation, Phys. Rev. Lett. **129,** 060501 (2022).

[51] I. Pietikäinen, S. Danilin, K. S. Kumar, A. Vepsäläinen, D. S. Golubev, J. Tuorila, and G. S. Paraoanu, Observation of the Bloch-Siegert shift in a driven quantum-to-classical transition, Phys. Rev. B **96,** 020501(R) (2017).

[52] B. Ann, W. Kessels, and G. A. Steele, Sideband interactions in a two-mode Josephson circuit driven beyond the rotating-wave approximation, Phys. Rev. Res. **3,** 033004 (2021).

[53] Yaxing Zhang, Jacob C. Curtis, Christopher S. Wang, R. J. Schoelkopf, and S. M. Girvin, Drive-induced nonlinearities of cavity modes coupled to a transmon ancilla, Phys. Rev. A **105,** 022423 (2022).

[54] Jayameenakshi Venkatraman, Xu Xiao, Rodrigo G. Cortiñas, Alec Eickbusch, and Michel H. Devoret, Static effective Hamiltonian of a rapidly driven nonlinear system, Phys. Rev. Lett. **129,** 100601 (2022).

[55] Jayameenakshi Venkatraman, Xu Xiao, Rodrigo G. Cortiñas, and Michel H. Devoret, On the static effective Lindbladian of the squeezed Kerr oscillator, arXiv:2209 .11193.

[56] Ross Shillito, Alexandru Petrescu, Joachim Cohen, Jackson Beall, Markus Hauru, Martin Ganahl, Adam G.M. Lewis, Guifre Vidal, and Alexandre Blais, Dynamics of transmon ionization, Phys. Rev. Appl. **18,** 034031 (2022).

[57] Joachim Cohen, Alexandru Petrescu, Ross Shillito, and Alexandre Blais, Reminiscence of classical chaos in driven transmons, Phys. Rev. X **4,** 020312 (2023).

[58] Moein Malekakhlagh, Alexandru Petrescu, and Hakan E. Türeci, Lifetime renormalization of weakly anharmonic superconducting qubits: I. Role of number non-conserving terms, Phys. Rev. B **101,** 134509 (2020).

[59] Moein Malekakhlagh, Alexandru Petrescu, and Hakan E. Türeci, Lifetime renormalization of driven weakly anharmonic superconducting qubits. II. The readout problem, Phys. Rev. B **129,** 134510 (2020).

[60] Alexandru Petrescu, Camille Le Calonnec, Catherine Leroux, Agustin Di Paolo, Pranav Mundada, Sara Sussman, Andrei Vrajitoarea, Andrew A. Houck, and Alexandre Blais, Accurate methods for the analysis of strong-drive effects in parametric gates, Phys. Rev. Appl. **19,** 044003 (2023).

[61] See Supplemental Material at http://link.aps.org/ supplemental/10.1103/PhysRevLett.131.193605 for detailed information on the theoretical derivation, numerical simulation method, device, experimental setup, and data acquisition process, which includes Refs. [61–68].

[62] D. J. Thoen, B. G. C. Bos, E. A. F. Haalebos, T. M. Klapwijk, J. J. A. Baselmans, and Akira Endo, Superconducting NbTiN thin films with highly uniform properties over a Ø 100 mm wafer, IEEE Trans. Appl. Supercond. **27,** 1 (2017).

[63] Y. Yan, Z. Lü, J. Luo, and H. Zheng, Effects of counter-rotating couplings of the Rabi model with frequency modulation, Phys. Rev. A **96,** 033802 (2017).

[64] I. Pietikäinen, S. Danilin, K. S. Kumar, A. Vepsäläinen, D. S. Golubev, J. Tuorila, and G. S. Paraoanu, Observation of the Bloch-Siegert shift in a driven quantum-to-classical transition, Phys. Rev. B **96,** 020501(R) (2017).

[65] J. R. Johansson, P. D. Nation, and F. Nori, QuTiP: An open-source PYTHON framework for the dynamics of open quantum systems, Comput. Phys. Commun. **183,** 1760 (2012).

[66] J. R. Johansson, P. D. Nation, and F. Nori, QuTiP 2: A PYTHON framework for the dynamics of open quantum systems, Comput. Phys. Commun. **184,** 1234 (2013).

[67] Markus Aspelmeyer, Tobias J. Kippenberg, and Florian Marquardt, Cavity optomechanics, Rev. Mod. Phys. **86,** 1391 (2014).

[68] B. Ann, Tunable quantum interfaces between superconducting qubits and microwave photons induced by extreme driving, TU Delft thesis, Delft University of Technology, 2021.

[69] Moein Malekakhlagh, Alexandru Petrescu, and Hakan E Türeci, Lifetime renormalization of driven weakly anharmonic superconducting qubits. II. The readout problem, Phys. Rev. B **129,** 134510 (2020).

[70] Jay Gambetta, Alexandre Blais, D. I. Schuster, A. Wallraff, L. Frunzio, J. Majer, M. H. Devoret, S. M. Girvin, and R. J. Schoelkopf, Qubit-photon interactions in a cavity: Measurement-induced dephasing and number splitting, Phys. Rev. A **74,** 042318 (2006).

[71] D. I. Schuster, A. Wallraff, A. Blais, L. Frunzio, R.-S. Huang, J. Majer, S. M. Girvin, and R. J. Schoelkopf, ac stark shift and dephasing of a superconducting qubit strongly coupled to a cavity field, Phys. Rev. Lett. **94,** 123602 (2005).

[72] B.-m. Ann, S. Deve, and G. A. Steele, Resolving nonperturbative renormalization of a microwave-dressed weakly anharmonic superconducting qubit, 10.5281/zenodo .7416976 (2022).